J. Neural Eng. **7** (2010) 056005 (10pp) doi:10.1088/1741-2560/7/5/056005

Design of a robust EMG sensing interface for pattern classification

He Huang[1], **Fan Zhang, Yan L Sun and Haibo He**

Department of Electrical, Computer, and Biomedical Engineering, University of Rhode Island, Kingston, RI 02881, USA

E-mail: huang@ele.uri.edu

Received 25 May 2010
Accepted for publication 4 August 2010
Published 1 September 2010
Online at stacks.iop.org/JNE/7/056005

Abstract

Electromyographic (EMG) pattern classification has been widely investigated for neural control of external devices in order to assist with movements of patients with motor deficits. Classification performance deteriorates due to inevitable disturbances to the sensor interface, which significantly challenges the clinical value of this technique. This study aimed to design a sensor fault detection (SFD) module in the sensor interface to provide reliable EMG pattern classification. This module monitored the recorded signals from individual EMG electrodes and performed a self-recovery strategy to recover the classification performance when one or more sensors were disturbed. To evaluate this design, we applied synthetic disturbances to EMG signals collected from leg muscles of able-bodied subjects and a subject with a transfemoral amputation and compared the accuracies for classifying transitions between different locomotion modes with and without the SFD module. The results showed that the SFD module maintained classification performance when one signal was distorted and recovered about 20% of classification accuracy when four signals were distorted simultaneously. The method was simple to implement. Additionally, these outcomes were observed for all subjects, including the leg amputee, which implies the promise of the designed sensor interface for providing a reliable neural–machine interface for artificial legs.

1. Introduction

Surface electromyographic (EMG) signals are one of the major neural control sources for powered prostheses, exoskeletons and rehabilitation robots (Basmajian and De Luca 1985). Various EMG signal-processing algorithms have been used to decipher user intent for neural control of external devices. Simple methods, such as computation of the root mean square (RMS) value, have been used to estimate the EMG magnitude. When the EMG magnitude is above a set value, the user's movement intent is identified; this triggers the control of external devices (Dipietro *et al* 2005, Williams 1990). EMG pattern classification or pattern recognition is an advanced signal processing method that has been investigated with promising results in the laboratory setting (Graupe *et al* 1982, Micera *et al* 1999, Englehart and Hudgins 2003, Ajiboye and Weir 2005, Chang *et al* 1996). Beyond the signal magnitude, a typical pattern recognition algorithm extracts a set of features that characterize the acquired EMG signals and then classifies the user's intended movement for external device control. The benefits of pattern classification are that it can extract more neural information with fewer monitored EMG signals than simple methods based only on the EMG magnitude (Zhou *et al* 2007).

EMG pattern classification has been investigated for neural control of upper-limb prostheses for decades (Englehart and Hudgins 2003, Micera *et al* 1999, Hudgins *et al* 1993, Graupe *et al* 1982); however, no EMG-controlled lower limb prostheses are commercially available. Recently, the need for neural control of computerized prosthetic legs has brought the idea of EMG-based control back to our attention. One of the challenges in using EMG pattern recognition methods originally designed for prosthetic arm control (Englehart and Hudgins 2003) is that the recorded EMG signals from lower limbs in each locomotion mode (class) are time varying (Huang *et al* 2009), while the EMG signals collected during

[1] Author to whom any correspondence should be addressed.

one type of constant force upper limb movement (class) are stationary. To address this difficulty, a new phase-dependent pattern classification strategy was designed (Huang *et al* 2009). By assuming that the EMG signals in a short gait phase are quasi-stationary and have a repeatable pattern for the same locomotion mode, we built one classifier, similar to the EMG pattern recognition methods for upper limb prosthesis, for each defined gait phase. This dynamic pattern recognition strategy allowed accurate classification of six locomotion modes when the input EMG signals were collected from the gluteal and thigh muscles of able-bodied subjects and patients with long transfemoral amputations (Huang *et al* 2009). This result indicated the potential of a phase-dependent pattern classification system for neural control of artificial legs. In addition, since current design of powered artificial legs uses varied impedance control according to gait phases (Martinez-Villalpando and Herr 2009, Varol *et al* 2010), the phase-dependent EMG pattern recognition for user intent identification can be easily integrated with the mechanical control scheme.

Another challenge in the design of EMG-controlled artificial legs is the unreliability of EMG recordings from leg muscles over time. Although EMG pattern classifiers previously designed for prosthetic arms or legs produced high accuracy for identifying user intent in single-session experiments (Englehart and Hudgins 2003, Micera *et al* 1999, Hudgins *et al* 1993, Graupe *et al* 1982, Huang *et al* 2009), their robustness during long-term prosthesis use has rarely been evaluated (Zecca *et al* 2002). In EMG-controlled artificial arms, environmental noise, electrode conductivity changes, sensor (electrode) location shifts or loss of electrode contact were reported to cause disturbances in recorded EMG signals and even damage to EMG electrodes (Parker *et al* 2006, Hargrove *et al* 2007, Sensinger *et al* 2009). The number of occurrences and the magnitude of these disturbances are amplified in the EMG electrode interface for prosthetic legs because of the constant, dynamic motion of the lower limbs. Since pattern recognition involves learning the muscle contraction patterns for intended movements and does not accommodate changes in EMG signals, these disturbances threaten the stability of EMG pattern classification performance and may even lead to system failure (Sensinger *et al* 2009). This significantly challenges the clinical application of EMG pattern classification for neural control of artificial limbs. It is especially problematic for artificial leg control because system failure may directly cause the user to fall and suffer serious injuries. Hence, the need for improved robustness of the sensor interface and reliability of EMG pattern classification takes on even greater importance for the design of neurally controlled artificial legs.

To make the EMG pattern classification method clinically viable, engineers have developed various potential solutions, such as physically stabilizing the EMG electrode contact, using concentric EMG electrodes (Disselhorst-Klug *et al* 1997, van Vugt and van Dijk 2001) and developing adaptive pattern classifiers (Sensinger *et al* 2009). Stabilizing EMG electrodes or using concentric electrodes rather than bipolar electrodes may make the sensor interface robust with respect to some causes of signal disturbances, such as changes in the inter-pole distance of bipolar electrodes, but not with respect to others. Adaptive pattern recognition is a promising method that may maintain the performance of the classifier over time when the recorded EMG signals change due to various causes (Sensinger *et al* 2009, Nishikawa *et al* 2000, Fukuda *et al* 2003). However, the method is difficult to implement in clinics because supervised adaptation requires frequent retraining sessions with the user, and unsupervised adaptation has not been shown to significantly improve system performance due to frequent uncertainty of the correct class (Sensinger *et al* 2009).

In this study, we aimed to improve the reliability of EMG pattern recognition by designing a robust EMG sensor interface. An additional module, called a sensor fault detection (SFD) module, was placed between the EMG electrodes and the pattern classifier. This module not only closely monitored the recordings from individual EMG electrodes, but recovered the classification performance of the system when one or more signals were disturbed. Such a design can improve system reliability regardless of the cause of the disturbance and is easy to implement for clinical practice. We evaluated this design on a phase-dependent pattern classifier that identified the user's intended transitions between different locomotion modes. Our engineering effort could inform the design of clinically viable EMG pattern classification systems and shows the potential application of this method for the design of a reliable neural–machine interface for artificial legs based on EMG pattern classification.

2. Methods

2.1. Participants and data collection

This study was conducted with Institutional Review Board (IRB) approval and informed consent of all subjects. Five able-bodied subjects (two males and three females; subjects AB1–AB5), free from orthopedic or neurological pathologies, and one male subject with a long, unilateral transfemoral (TF) amputation (subject TF1) were recruited. The average age of able-bodied subjects was 42.4 ± 14.5 years. The recruited amputee subject was 51 years old and 32 years post-amputation. The ratio of the length of the residual limb (measured from the greater trochanter to the amputation site) to the thigh length on the non-impaired side (measured from the greater trochanter to the lateral epicondyle) was 0.82.

Ten surface EMG signals from gluteal and thigh muscles were collected from able-bodied subjects. The monitored muscles included the gluteus maximus (GMA), gluteus medius (GME), sartorius (SAR), rectus femoris (RF), vastus lateralis (VL), vastus medialis (VM), gracilis (GRA), biceps femoris long head (BFL), semitendinosus (SEM) and biceps femoris short head (BFS). The bipolar EMG electrodes (i.e. sensors) were placed over the anatomical locations described by Perotto and Delagi (Perotto *et al* 2005). For the amputee subject, an additional muscle, adductor magnus (ADM), was monitored from the residual limb, and therefore, 11 EMG signals were recorded. It is noteworthy that the locations of the EMG

electrodes on the thigh muscles of the amputee subject were approximate.

Active surface EMG electrodes were used in this study. The electrodes contained a pre-amplifier that band-pass filtered the EMG signals between 20 and 3000 Hz with a pass-band gain of 20. The electrodes (MA-411-002, Motion Lab System Inc., Baton Rouge, LA) consisted of two contacts and were directly attached to the skin surface of the able-bodied subjects. For the amputee subject, EMG electrodes were mounted on an experimental socket with electrode contact domes (Liberating Technologies, Inc., Holliston, MA), which can penetrate the experimental socket for reliable electrode–skin contact. Before electrode placement or socket donning, the skin was shaved and cleaned. A ground electrode was placed on the bony part of the knee for able-bodied subjects and near the anterior iliac spine for the amputee subject.

Gait events were detected by force-sensitive resistor (FSR)-based footswitches placed under the tested foot and via motion data of light reflective markers placed over the heel and toe. A data collection system (MA-300-16, Motion Lab System Inc., Baton Rouge, LA) collected 10 or 11 channels of EMG data and footswitch data simultaneously. The cut-off frequency of the anti-aliasing filter was 500 Hz for EMG data and 120 Hz for footswitch data. Both sources were then digitally sampled at a rate of 1440 Hz. The marker positions were captured by six motion-tracking cameras (Motion Analysis Corp., Santa Rosa, CA) and sampled at 120 Hz. All recordings were synchronized.

2.2. Experimental protocol

In the experiment, the able-bodied subjects wore their own walking shoes, and the TF subject wore his own prosthesis (a Mauch® SNS knee and a 27 cm Vari-Flex® foot). The TF subject's experimental socket was duplicated from his own ischial containment socket with suction suspension. In addition, a total elastic suspension belt was used to reinforce socket suspension. Each subject was instructed to perform four locomotion modes: level-ground walking, ascending stairs, descending stairs and stepping over an obstacle. Level-ground walking was conducted on a straight walkway 9 m long. Subjects were instructed to walk at a comfortable speed. A three-stair staircase was used for stair ascent and stair descent tests. The staircase was 20 cm high, 75 cm wide and 26 cm deep. In the trials for ascending stairs, the subjects walked on level ground toward the staircase and then performed stair ascent. For the task of stair descent, the subjects performed stair descent first and then level ground walking. For the task of stepping over an obstacle, the subjects were asked to step over a box (19 cm high, 30 cm wide and 10 cm deep) during ambulation.

Subjects performed only one type of task in each trial. Each locomotion transition was repeated at least ten times. The order of the tasks was randomly assigned. Rest periods were allowed between trials to avoid fatigue.

2.3. EMG pattern recognition algorithm

One of the motivations for this study was to achieve neural control of artificial legs; therefore, the designed sensor interface was tested on a phase-dependent EMG pattern classifier—a potential design of a neural–machine interface for prosthetic legs (Huang *et al* 2009). In this study, transitions between locomotion modes were considered to occur in the gait phase 200 ms prior to the toe-off event. The goal of the pattern classification system was to accurately identify the transitions from level walking to stair ascent, from stair decent to level walking, from level walking to stepping over an obstacle, and level walking only (i.e. no transition). The pre-swing phase was selected as the transition phase because precise decisions in this phase are critical for allowing the prosthesis controller to adjust the knee impedance or position during the swing phase to clear the prosthetic foot from the staircase or obstacle.

The raw EMG data were band-pass filtered between 25 and 450 Hz by a digital, eighth-order Butterworth filter to remove low-frequency motion artifacts and high-frequency noise. EMG data collected in the 200 ms immediately prior to toe-off (PTO) during task transition steps were selected for analysis. Overlapped analysis windows were used in each PTO phase. The analysis window was 100 ms in duration and slid with a 50 ms increment. Hence, there was a total of three analysis windows in each PTO phase. Four time-domain (TD) features (mean absolute value, number of zero-crossings, waveform length and number of slope sign changes (Hudgins *et al* 1993)) of EMG signals were extracted from each analysis window as $\bar{f}_n$, where n denotes the EMG channel number. A feature vector ($\bar{F}$) in one analysis window was then formulated as $\bar{F} = \{\bar{f}_1, \bar{f}_2, \bar{f}_3, \ldots, \bar{f}_N\}$, where N denotes the total number of EMG channels. Three feature vectors were extracted from the EMG signals in one PTO phase. A simple linear discriminant analysis (LDA)-based classifier was used because it is computationally efficient in real-time prosthesis control and has similar classification performance as other more complex classifiers (Englehart and Hudgins 2003, Huang *et al* 2009). Due to the relatively small number of collected transitional gait cycles, leave-one-out cross-validation (LOOCV) was utilized in order to receive a precise estimation of the classification accuracy. In the LOOCV procedure, the features extracted from one PTO phase were used as the testing data, and the remaining features were used as the training data. This procedure was repeated so that EMG signals in each PTO phase were used once as the testing data. To evaluate the performance of the classifier, the overall classification accuracy (CA) was calculated:

$$\mathrm{CA} = \frac{\text{Number of Correct Classification Decisions}}{\text{Total Number of Classification Decisions}} \times 100\%. \quad (1)$$

2.4. Sensor fault detector and system self-recovery strategy

In order to further improve the robustness of the EMG pattern classification system, a sensor fault detection (SFD) module, composed of sensor fault detectors and a system self-recovery strategy, was designed. The block diagram of the module is shown in figure 1. In each analysis window, the detection module received the features extracted from individual EMG signals as input. One sensor fault detector was designed

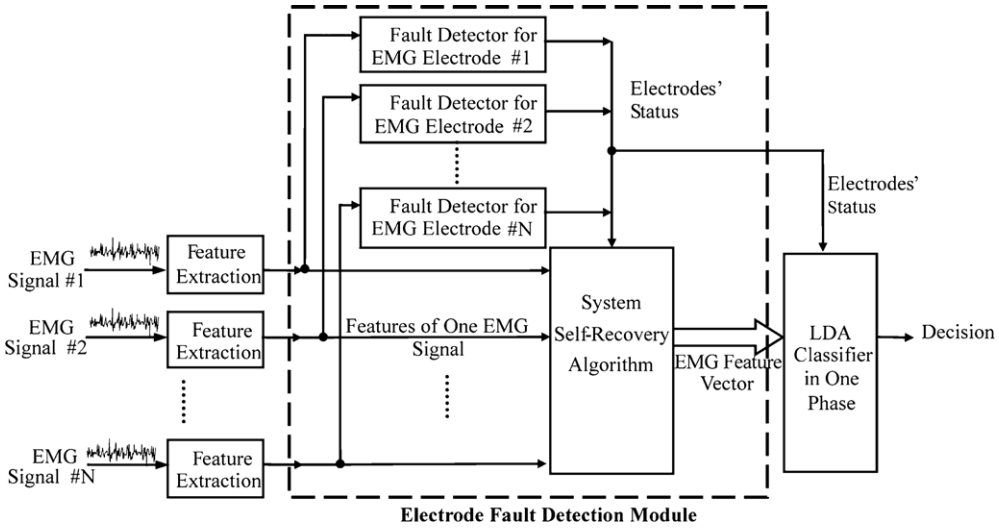

Figure 1. Block diagram of the EMG pattern recognition system with a sensor fault detection module.

in the detection module based on the distribution of EMG features extracted from each EMG electrode recording. The status of each EMG electrode (either with or without abnormal recordings) was reported to a system self-recovery algorithm that reduced or compensated for the influence of abnormal sensors on the performance of EMG pattern classification.

2.4.1. Sensor fault detector based on Bayesian decision rule. Three types of signal distortions were considered in this study: EMG signal drift and saturation, additional noise in the signal and variation of EMG magnitude. In addition, magnitude changes were further separated into magnitude increases and magnitude decreases. In this study, the behavior of the associated sensors was considered abnormal when the signal disturbance caused a more than 5% decrease in classification accuracy compared to the accuracy when no signal was disturbed. The function of the sensor fault detector was to detect these abnormal EMG recordings. This definition of normal/abnormal signals was based on the criteria that a $\geqslant$5% decrease in classification accuracy demonstrates a deterioration of the system performance, while the disturbance that causes $<$5% accuracy drop is deemed small enough without damaging the system performance. Note that these criteria were based on the previous experiences of using EMG pattern recognition to drive a virtual arm and were rather subjective; thresholds other than 5% accuracy decrease can be used to define the behavior of sensors and are dependent on the requirement of classification system design.

The Bayesian detection criterion was used to design the sensor fault detector for each EMG electrode because it is effective and can minimize the probability of detection error (Kay 1998). Since four types of signal distortions were considered in this study, the detection task consisted of testing five hypotheses (Van Trees 1968): H_0: the recorded signal is normal, H_1: the signal is abnormal and contains signal drift and saturation, H_2: the signal is abnormal and contains additional noise, H_3: the signal is abnormal and contains a signal magnitude increase and H_4: the signal is abnormal and contains a signal magnitude decrease. The five-hypothesis Bayesian risk function is expressed as

$$\Re = \sum_{i=0}^{M-1}\sum_{j=0}^{M-1} P_j C_{ij} \int_{Z_i} p(R|H_j)\,\mathrm{d}R, \qquad (M=5), \quad (2)$$

where P_j denotes the prior probabilities of each hypothesis; z_i represents the observation space of each hypothesis; R denotes the observed EMG feature vector, composed of four TD features; C_{ij} is the cost coefficient assigned to the decision that chooses H_i when H_j is true and $p(R|H_j)$ is the likelihood function. The likelihood function was modeled as a multivariable normal distribution (MVN):

$$p(R|H_j) = \frac{1}{(2\pi)^{d/2}|\Sigma_j|^{\frac{1}{2}}} \times \exp\left\{-\frac{1}{2}(R-\mu_j)^T \Sigma_j^{-1}(R-\mu_j)\right\}, \quad (3)$$

where μ_j and Σ_j are the mean vector and covariance matrix of hypothesis j, respectively and d denotes the dimension of feature vector R ($d=4$ in this study). The goal of the Bayesian detector is to provide the decision rule so that, on average, the risk as defined in (2) will be as small as possible.

Two assumptions were made in this study: (1) the prior probabilities of the four signal faults (P_1, P_2, P_3 and P_4) were assumed to be equal and were denoted as P, and therefore, the prior probability P_0 of hypothesis H_0 was (1–4P); and (2) the cost coefficient C_{ij} was defined as follows:

$$C_{ij} = \begin{cases} 0, \text{ when } i = j \text{ or } i, \quad j \neq 0 \\ C_{\mathrm{TF}}, \text{ when } i = 0 \quad \text{and} \quad j \neq 0 \\ C_{\mathrm{FT}}, \text{ when } j = 0 \quad \text{and} \quad i \neq 0, \end{cases} \quad (4)$$

where C_{FT} denotes the cost coefficient assigned to the decision when a normal signal is incorrectly identified as abnormal, while C_{TF} represents the cost coefficient assigned when the detector fails to recognize a faulty signal. According to these

assumptions, the Bayes decision criterion can be expressed as

$$\frac{p(R|H_1)}{p(R|H_0)} + \frac{p(R|H_2)}{p(R|H_0)} + \frac{p(R|H_3)}{p(R|H_0)} + \frac{p(R|H_4)}{p(R|H_0)} \underset{\text{normal signal}}{\overset{\text{abnormal signal}}{\gtrless}} \frac{1-4P}{P} \cdot \frac{C_{\text{FT}}}{C_{\text{TF}}}, \tag{5}$$

where $\frac{1-4P}{P} \cdot \frac{C_{\text{FT}}}{C_{\text{TF}}}$ is defined as the threshold of the Bayesian detector. If the value on the left side of (5) was greater than the detection threshold, the current EMG recording was detected as an abnormal one; otherwise, it was considered as a normal signal.

One fault detector was designed for each EMG electrode (figure 1). The likelihood $p(R|H_j)$ on the left side of equation (5) was estimated based on half the collected data (for $j = 0$) or data with simulated disturbances (for $j = 1, 2, 3$ or 4) from one electrode during all studied locomotion transitions. In this study, signal disturbances causing more than a 5% decrease in classification accuracy were considered abnormal and applied to simulate the distorted signals. The rest of the data or simulated data were applied to evaluate the detection performance. The receiver operating characteristic (ROC) curve for each electrode's fault detector was computed to determine the optimal threshold. To optimize the performance of the detector, the threshold was determined by minimizing $\sqrt{(1-\text{sensitivity})^2 + (1-\text{specificity})^2}$, where the *sensitivity* of the detector was the proportion of correctly detected abnormal signals out of all the abnormal cases tested, and the *specificity* of the detector was the proportion of correctly identified normal signals out of all the normal EMG signals tested. The optimal operating point on the ROC curve is at the upper-left corner, where both sensitivity and specificity are equally maximized.

2.4.2. System self-recovery strategy. Beyond detection of abnormal sensor behavior, the design of a self-recovery method to 'fix' the system in the presence of abnormal EMG signals is essential for ensuring reliable EMG pattern classification. Our previous study (Huang *et al* 2009) demonstrated that the information recorded from 10 gluteal and thigh muscles was redundant because the EMG classification performance was not significantly affected by the removal of one or two EMG signals. This situation makes the design of a system self-recovery strategy possible. In the present study, the self-recovery method made use of information redundancy and simply removed EMG signals from the input of the classifier when they were detected as 'abnormal'. The system self-recovery method (figure 1) modified the EMG feature vector by eliminating the four EMG features from failed sensors. In addition, the classifier was retrained automatically based on the stored EMG features extracted from the original training data of the remaining 'normal' channels. Then the modified EMG feature vector was sent into the retrained classifier as an input for pattern recognition. Note that in real-time application this method does not require recollecting the training data, but needs to store the EMG features extracted from the initial training data.

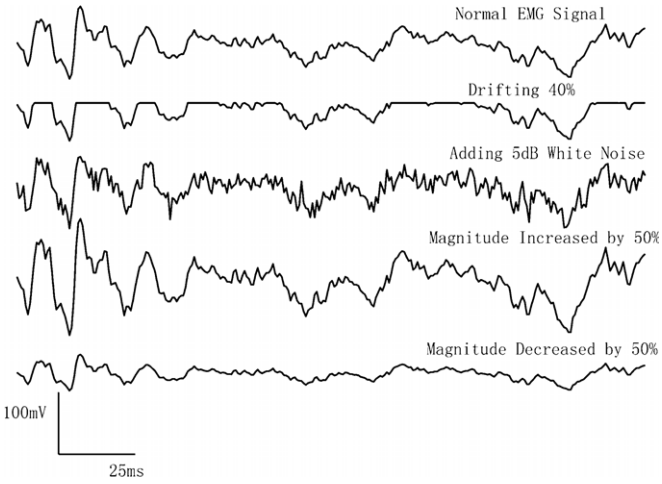

Figure 2. Examples of 200 ms of simulated EMG signals with different distortions.

2.5. Evaluation of sensor fault detection

2.5.1. Disturbance simulation. The magnitude, environmental noise and/or baseline of one or more EMG channels were artificially adjusted to simulate the different disturbances commonly occurring at the sensor interface.

(1) *Signal baseline drift and saturation*: one common disturbance of EMG recordings is motion artifacts (Basmajian and De Luca 1985, Parker *et al* 2006), which lead to drifts in EMG magnitude from baseline. Although low-frequency components can be removed by a high-pass filter when the drifts are small, EMG signals can be significantly distorted by considerable drifts that cause the signal magnitude to saturate. In this case, EMG signal information can be lost, which eventually affects the classification accuracy of the EMG pattern recognition system. Signal saturation is also observed when EMG electrodes lose contact with the skin. In this study, drift and saturation of EMG signals were simulated by

$$\begin{cases} y(i) = a \cdot \text{PP}(y), & \text{if } y(i) \geqslant a \cdot \text{PP}(y) \\ y(i) = y(i), & \text{if } y(i) < a \cdot \text{PP}(y), \end{cases} \tag{6}$$

where $y(i)$ is the EMG signal recorded from one electrode; PP(y) denotes the peak-to-peak magnitude of EMG signal $y(i)$ recorded in the experiment and a is the signal drift level that ranges from 5 to 50% of PP(y). Different levels of EMG distortion were simulated by adjusting the value of a. When a equaled 50%, around half of the signal information was lost. An example of a simulated EMG signal with this distortion is demonstrated in figure 2. The EMG information was completely lost at the flat data segments, which resulted from the data saturation.

(2) *Noise*: thermal noise or coupled environmental noise often affects the surface EMG electrode interface (Lopez *et al* 2009, Huigen *et al* 2002). The noise was simulated by adding synthetic white Gaussian noise (WGN) that resulted in different signal-to-noise ratios (SNRs). The SNRs ranged from 20 dB (low noise level) to 0 dB (high noise level) (Phinyomark *et al* 2009). An example of an EMG signal with additional 5 dB synthetic noise is shown in figure 2.

(3) *Variation of EMG signal magnitude*: shifts in EMG electrode locations, changes to bipolar electrode orientations and altered inter-pole distances cause significant variations in the EMG signal magnitude (Vigreux *et al* 1979). This is coupled with frequency-component changes. In this study we simply increased and decreased the magnitude of the EMG signals (figure 2) to simulate disturbances due to changing EMG electrode location, orientation and/or configuration. The variations of the EMG signal magnitude were simulated by

$$y(i) = (1 + a) \cdot y(i), \tag{7}$$

where $y(i)$ is a EMG signal; a is the signal magnitude variation level that ranges from 10 to 100% for magnitude increase and −10% to −95% for magnitude decrease.

2.5.2. Evaluation of designed sensor fault detection. The ROC curve was one of the metrics used to evaluate the designed sensor fault detectors. In addition, the detection accuracy rate for individual disturbances was used to quantify the accuracy of the sensor fault detector in identifying signal disturbances of varying levels. It was defined as the percentage of correct decisions made in all tested analysis windows. Note that EMG signals with any level of disturbance were considered distorted signals when calculating the detection accuracy rate for signal disturbances, while EMG signals with disturbances that caused more than a 5% drop in classification accuracy were defined as abnormal signals for generation of the ROC curve.

To evaluate the SFD module, one or more EMG signals in the testing data set were artificially distorted and then used to test the overall accuracy of the EMG classification system with and without the SFD module. The difference in classification accuracy with and without the designed module was used to quantify the effect of the SFD module on the reliability of the EMG pattern classification system.

3. Results

3.1. Receiver operating characteristic (ROC) curve

Figure 3 shows the representative ROC curves of 11 fault detectors designed for individual EMG channels for subject TF1. When the sensitivity and specificity were set to 0.8, multiple operating points on each ROC curve were to the upper-left side of this marker. This means that over 80% sensitivity and specificity could be achieved for the optimally designed fault detector for each EMG channel. This fault detector used the threshold resulting from the furthest upper-left corner of the ROC curve. In addition, the performance of each detector was not very sensitive to the selected threshold because the operating point remained within the upper-left region of the ROC curve (greater than 0.8 sensitivity and specificity) even with moderate shifts in the selected operating point. Similar patterns were also obtained for the ROC curves of the designed detectors for all able-bodied subjects (AB1–AB5).

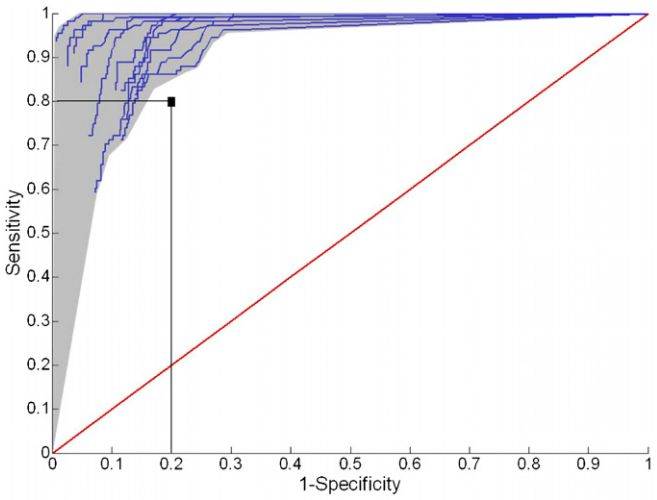

Figure 3. Representative ROC curves of 11 sensor fault detectors from subject TF1. The vertical axis denotes sensitivity, i.e. the ratio of true positives. The horizontal axis denotes (1 – specificity), i.e. the ratio of false positives.

(This figure is in colour only in the electronic version)

3.2. System performance with one distorted EMG signal

Figure 4 shows the detection accuracy rate of the sensor fault detector for different disturbances and compares the performance of the EMG classification system with and without the SFD module. The represented detector was designed for the channel that recorded EMG signals from the RF of TF1. When the level of distortion applied to one signal increased, the detection accuracy rate for signal disturbances increased, the classification accuracy achieved without the SFD module decreased and the classification performance of the system with the SFD module was not influenced. Compared to the accuracy of the classification system without the SFD module, the system accuracy with the module recovered by at least 5% when the signal was distorted by greater than 37% baseline drift, more than 9 dB white noise, greater than 60% magnitude increase or greater than 40% magnitude decrease.

Similar results were observed for all other EMG channels and for able-bodied subjects. Figure 5 shows the average classification accuracies across five able-bodied subjects when individual monitored EMG channels were disturbed. The levels of simulated signal distortions were fixed across subject. The system with the SFD module produced higher classification accuracy than the system without it. In addition, this difference reached statistical significance ($p < 0.05$, one-way ANOVA) for the GMA, SAR and VL muscles with 40% baseline drift; the RF and VM muscles with 5 dB additional white noise; the RF and BFL muscles with 50% amplitude increases and the RF muscle with a 50% amplitude decrease. Note that the differences in system accuracies with and without the SFD module depended on the level of signal distortion; these differences increased when the disturbance levels increased.

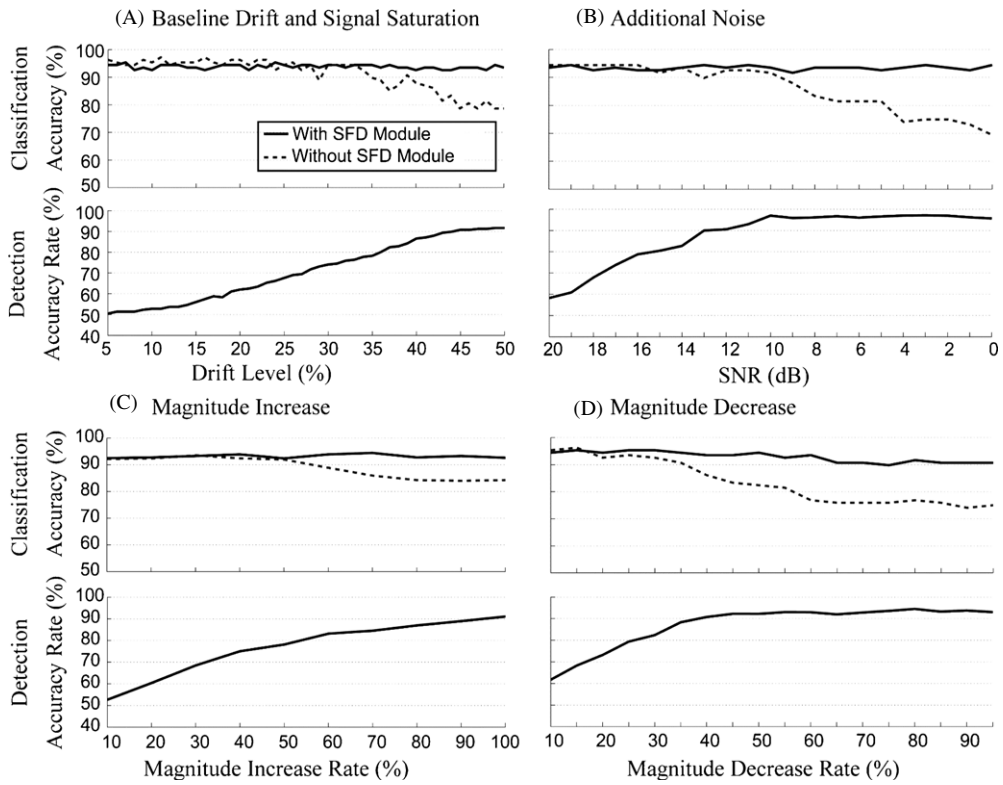

Figure 4. The classification accuracy of the system with and without the sensor fault detection module for increasing signal distortion levels (upper panel of each subplot) and the detection accuracy rate of the designed sensor fault detector for increasing signal distortion levels (lower panel of each subplot). These representative results were derived from the EMG signals recorded from the rectus femoris of TF1.

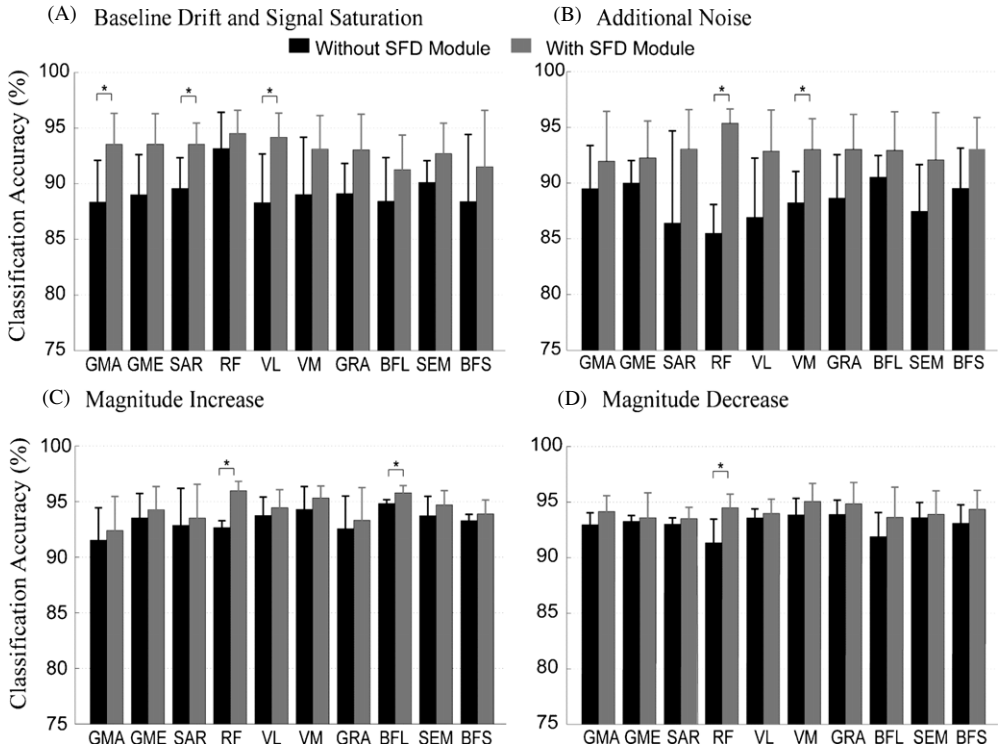

Figure 5. Comparison of average classification accuracy of the systems with (gray bars) and without (black bars) the sensor fault detectors and self-recovery strategy. The classification accuracies were averaged across five able-bodied subjects when individual signals were disturbed. The level of signal drift, SNR of added white noise, percentage of magnitude increase and percentage of magnitude decrease were set to 40%, 5 dB, 50% and 50%, respectively. * denotes statistical significance ($P < 0.05$, one-way ANOVA) between the accuracy of the system with and without the SFD module.

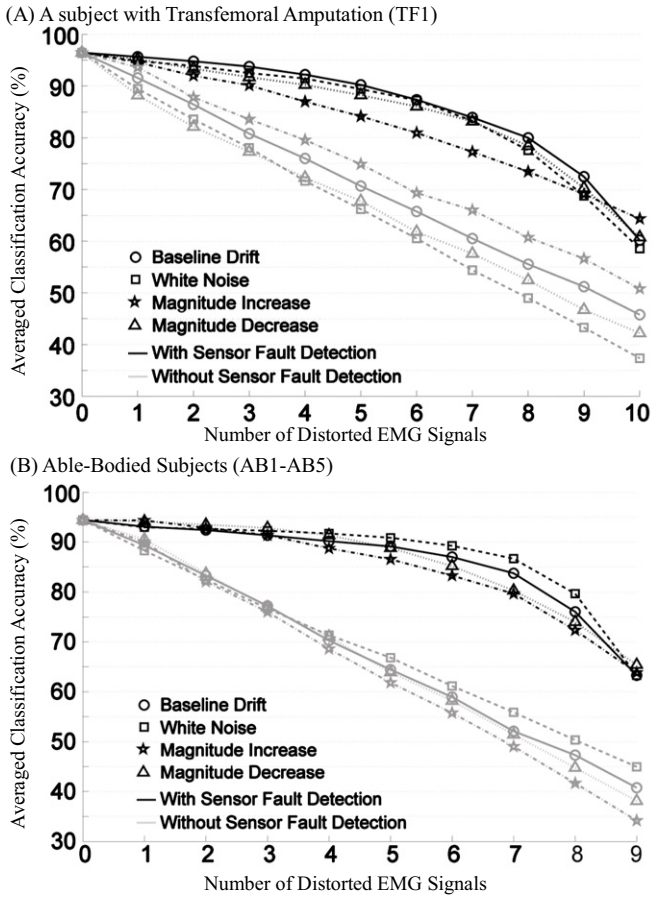

Figure 6. Average classification accuracy of the system with (black lines) and without (gray lines) the sensor fault detection module as the number of distorted signals increased. (A) The classification accuracy averaged across different combinations of abnormal electrodes for subject TF1. (B) The classification accuracy averaged across combinations of abnormal electrodes and across five able-bodied subjects (AB1–AB5). The level of signal drift, SNR of added white noise, percentage of magnitude increase and percentage of magnitude decrease were set to 40%, 5 dB, 50% and 50%, respectively.

3.3. System performance with multiple distorted EMG signals

The classification performance of the system deteriorated when the number of distorted signals increased, whether or not the SFD module was used (figure 6). However, the performance of the system with the SFD module deteriorated much more slowly than the system without the module. The differences in classification accuracy between the two systems generally increased with the number of distorted signals. This indicates that the benefit of the SFD module became more obvious when multiple channels of signals were disturbed at the same time. For example, when four EMG signals were simultaneously disturbed, the accuracy of the system without the SFD module dropped to around 75% for TF1 and to an average of 70% for able-bodied subjects, but was about 90% for the system with the SFD module. This demonstrated that the designed sensor fault detectors and self-recovery strategy could salvage system performance by up to 20% classification accuracy. It is noteworthy that the classification accuracies derived from the system with the SFD module (black lines in figure 6) were not significantly affected by the disturbance levels within the range simulated in this study.

4. Discussion

Disturbances in EMG recordings commonly cause unreliability in neural–machine interfaces based on EMG pattern classification. These problems are significant for EMG recordings from lower limbs because of the constant, dynamic motions of the legs. Since errors in the neural–machine interface for prosthetic legs may cause falls and serious injuries in the amputee users, improving the reliability of the interface is necessary before its real application. To address this challenge and make EMG pattern recognition clinically viable for neural control of artificial legs, we designed a robust EMG sensor interface with an SFD module and evaluated the design on a phase-dependent classifier for identifying transitions between locomotion modes.

The designed SFD module can ‘rescue’ the classification system from failure when one or more sensors record abnormal EMG signals. Using the designed SFD module, we found that the accuracy for classifying four mode transitions was stable regardless of the level of simulated disturbances in one EMG signal. This is because low-level disturbances, though difficult to detect, had a small impact on pattern classification, while high-level disturbances were easily detected and removed from the input to the classifier, which maintained performance due to the redundancy in the system inputs. The benefit of the designed SFD module became significant when the number of distorted EMG signals and the level of disturbance increased. Additionally, these promising results were observed for able-bodied subjects and a subject with a long transfemoral amputation. Therefore, the designed SFD module has great potential to improve the reliability of EMG pattern classification systems for artificial legs.

Information redundancy in collected EMG signals is essential for designing a robust EMG sensor interface and an efficient system self-recovery strategy. This is because the information loss must be compensated for by the redundancy in the monitored information in order to save the system from failure. A similar idea was demonstrated by previous studies (Lopez *et al* 2009, Hargrove *et al* 2006) in which the authors recorded redundant EMG information for a robust EMG-based neural–machine interface by placing multiple electrodes on the same muscle region. In our study, the redundancy was introduced by monitoring EMG signals from almost all of the surface gluteal and thigh muscles on one side of the leg or residual limb, as our previous study (Huang *et al* 2009) demonstrated the redundancy in the extracted EMG information for classifying the six locomotion modes using the same EMG electrode placement. If fewer than half of the recorded EMG signals were distorted, the information redundancy could compensate for part of the information loss and could still permit a functional classification system. In this case, our designed system can automatically update the classifier’s parameters with initially collected training data from undisturbed sensors; no retraining data are required. Therefore, compared to methods that

require frequent retraining for improved robustness in EMG pattern classification, this approach is easy and practical. If a greater number of EMG sensors were disturbed, the redundant information would be inadequate to 'rescue' the system based on the designed self-recovery method. In this case, the user may need to manually retrain the EMG pattern classifier or fix the failed sensor for continued use of the system.

The redundant information recorded from able-bodied subjects was more than that recorded from the subject with a long transfemoral amputation (TF1). This was determined from the ability of the system to maintain 85% classification accuracy with up to 5 out of 10 distorted signals for AB1–AB5, but only up to 4 out of 11 distorted signals for TF1. This implies reduced neural innervation or inactivity of leg muscles in the amputee due to amputation. In patients with short transfemoral or higher level amputations, the distal thigh muscles are missing; the amount of extractable neural information from EMG signals from the residual muscles is further limited in these cases. Therefore, use of our sensor interface for robust pattern classification may be challenging for these patients. An advanced surgical technique called targeted muscle reinnervation (TMR) (Kuiken *et al* 2004) is a promising method for solving this problem. During TMR surgery, the residual nerves that originally commanded the muscles in the missing limb are transferred to alternative residual muscles. After successful motor reinnervation, voluntary neural control signals propagate along the efferent nerves and activate these residual muscles. The resultant EMG signals contain the neural control information for the missing limb (Kuiken *et al* 2004, Kuiken 2006). Hence, TMR could enhance the information redundancy in recorded EMG signals and make our designed sensor interface and classification system applicable to patients with high-level lower limb amputations.

The sensor fault detectors and system self-recovery method designed in this study are relatively simple and adequate to correct for sudden signal disturbances simulated in the present study. In addition, the results of this study determine the levels of signal disturbances that deteriorate the offline performance of our designed classifier for locomotion mode identification. In real application these disturbance levels can be directly simulated to build the abnormal data models (i.e. hypotheses H_1–H_4 in this study) in the sensor fault detector design. However, it is inadequate to determine the clinical value of the designed SFD and pattern classification system for artificial legs merely based on this offline analysis. Generally, the high classification accuracy in offline analysis yields better classification performance in real time (Li *et al* 2010). Nevertheless, a very limited number of studies have been found on investigating the correlation between the EMG classification accuracy during offline analysis and the performance of EMG classification system during clinical applications. One recent study (Hargrove *et al* 2010) compared the LDA-based EMG classifier with the multiple binary classifier (MBC) for performing a functional task (i.e. transferring clothespins from a high vertical bar to a lower horizontal bar in a virtual environment). Interestingly, although LDA outperformed MBC in offline analysis by ∼3% accuracy, the subjects needed more time to finish the task when using LDA than when using MBC. This was because the main errors for LDA in real-time and offline analysis were the misclassifications of hand open, which caused the subjects to accidentally drop the virtual clothespin with incomplete task performance. The authors concluded that the controllability of the EMG pattern classifier depends on the type of errors and assigned task. Since our application of EMG pattern classification was for artificial legs, different from previous applications, further studies on implementing the designed algorithm should quantify the clinical significance of designed SFD for prosthetic legs. Another study limitation is that there may be more forms of signal disturbances than those simulated in this study. To address this challenge, one of the solutions is to acquire prior knowledge about the major sources and levels of disturbances in our application and then build 'abnormal' models based on commonly occurring types of disturbances. Another potential solution is to design a fault detector without specifying the abnormal model. The idea of this method is to build a normal model only; any observation outside of a certain confidence region of the normal model is detected as an abnormal recording. In addition, we did not consider gradual signal disturbances. The proposed system structure is feasible for detecting gradual changes when combined with the theory and methods of trust management (Jsang *et al* 2007, Sun *et al* 2006). The idea of trust establishment theory is to assign a continuous trust value to each sensor instead of a binary detection result (normal or abnormal). The trust information can be used to indicate gradual changes in signals and reduce the impact of untrustworthy sensors on system performance even before the sensors are detected as abnormal. Furthermore, the evaluation of the designed sensor interface was based on synthetic disturbances. Moreover, because the disturbances were simulated on the EMG signals in a short gait phase, the time response of the designed sensor fault detector was not considered. Additional efforts are needed to test the designed SFD with experimental induced disturbances on more leg amputees, integrate the SFD into a real-time EMG pattern classifier for locomotion mode identification and quantify the benefit of our designed SFD for improved reliability of the neural–machine interface for artificial legs.

5. Conclusions

To make EMG pattern recognition practical and available to patients with motor deficits, real-world challenges that result in variations in EMG signals and systems that are unreliable for long-term use must be overcome. In this study, we aimed to address these challenges by designing a sensor fault detection module to monitor the behavior of individual EMG electrodes and recover the classification performance of the system by a self-recovery strategy when recorded EMG signals were distorted. The results of this study demonstrate several benefits of the designed sensor interface. (1) The designed sensor interface was adequate to correct for sudden signal disturbances simulated in the present study. (2) No frequent retraining session was required, which makes the system easy to apply. (3) The performance of the system

tested on the patient with a long transfemoral amputation was similar to that derived from able-bodied subjects, making the application of our design for neural control of artificial legs straightforward. These promising outcomes could inform the design of clinically viable EMG pattern recognition systems and eventually benefit individuals with motor deficits.

Acknowledgments

The authors thank Todd Kuiken, MD, PhD, and Robert Lipschutz, CP, at the Rehabilitation Institute of Chicago for their suggestions and assistance in this project and Aimee Schultz for editing the manuscript. This work was partially supported by the Department of Defense (DoD)/TATRC #W81XWH-09-2-0020, the National Science Foundation (NSF)/CPS #0931820, National Institutes of Health (NIH)/NICHD #RHD064968A, and the Department of Education/NIDRR #H133F080006.

References

Ajiboye A B and Weir R F 2005 A heuristic fuzzy logic approach to EMG pattern recognition for multifunctional prosthesis control *IEEE Trans. Neural Syst. Rehabil. Eng.* **13** 280–91

Basmajian J V and De Luca C J 1985 *Muscles Alive: Their Functions Revealed by Electromyography* (Baltimore, MD: Williams & Wilkins)

Chang G C, Kang W J, Luh J J, Cheng C K, Lai J S, Chen J J and Kuo T S 1996 Real-time implementation of electromyogram pattern recognition as a control command of man–machine interface *Med. Eng. Phys.* **18** 529–37

Dipietro L, Ferraro M, Palazzolo J J, Krebs H I, Volpe B T and Hogan N 2005 Customized interactive robotic treatment for stroke: EMG-triggered therapy *IEEE Trans. Neural Syst. Rehabil. Eng.* **13** 325–34

Disselhorst-Klug C, Silny J and Rau G 1997 Improvement of spatial resolution in surface-EMG: a theoretical and experimental comparison of different spatial filters *IEEE Trans. Biomed. Eng.* **44** 567–74

Englehart K and Hudgins B 2003 A robust, real-time control scheme for multifunction myoelectric control *IEEE Trans. Biomed. Eng.* **50** 848–54

Fukuda O, Tsuji T, Kaneko M and Otsuka A 2003 A human-assisting manipulator teleoperated by EMG signals and arm motions *IEEE Trans. Robot. Autom.* **19** 210–22

Graupe D, Salahi J and Kohn K H 1982 Multifunctional prosthesis and orthosis control via microcomputer identification of temporal pattern differences in single-site myoelectric signals *J. Biomed. Eng.* **4** 17–22

Hargrove L, Englehart K and Hudgins B 2006 The effect of electrode displacements on pattern recognition based myoelectric control *Conf. Proc. IEEE Eng. Med. Biol. Soc.* vol 1 2203–6

Hargrove L J, Englehart K and Hudgins B 2007 A comparison of surface and intramuscular myoelectric signal classification *IEEE Trans. Biomed. Eng.* **54** 847–53

Hargrove L J, Scheme E J, Englehart K B and Hudgins B S 2010 Multiple binary classifications via linear discriminant analysis for improved controllability of a powered prosthesis *IEEE Trans. Neural Syst. Rehabil. Eng.* **18** 49–57

Huang H, Kuiken T and Lipschutz R D 2009 A strategy for identifying locomotion modes using surface electromyography *IEEE Trans. Biomed. Eng.* **56** 65–73

Hudgins B, Parker P and Scott R N 1993 A new strategy for multifunction myoelectric control *IEEE Trans. Biomed. Eng.* **40** 82–94

Huigen E, Peper A and Grimbergen C A 2002 Investigation into the origin of the noise of surface electrodes *Med. Biol. Eng. Comput.* **40** 332–8

Jsang A, Ismail R and Boyd C 2007 A survey of trust and reputation systems for online service provision *Decis. Support Syst.* **43** 618–44

Kay S M 1998 *Fundamentals of Statistical Signal Processing, Volume II: Detection Theory* (Englewood Cliffs, NJ: Prentice-Hall)

Kuiken T 2006 Targeted reinnervation for improved prosthetic function *Phys. Med. Rehabil. Clin. N. Am.* **17** 1–13

Kuiken T A, Dumanian G A, Lipschutz R D, Miller L A and Stubblefield K A 2004 The use of targeted muscle reinnervation for improved myoelectric prosthesis control in a bilateral shoulder disarticulation amputee *Prosthet. Orthot. Int.* **28** 245–53

Li G, Schultz A E and Kuiken T A 2010 Quantifying pattern recognition-based myoelectric control of multifunctional transradial prostheses *IEEE Trans. Neural Syst. Rehabil. Eng.* **18** 185–92

Lopez N M, di Sciascio F, Soria C M and Valentinuzzi M E 2009 Robust EMG sensing system based on data fusion for myoelectric control of a robotic arm *Biomed. Eng. Online* **8** 5

Martinez-Villalpando E C and Herr H 2009 Agonist–antagonist active knee prosthesis: a preliminary study in level-ground walking *J. Rehabil. Res. Dev.* **46** 361–73

Micera S, Sabatini A M, Dario P and Rossi B 1999 A hybrid approach to EMG pattern analysis for classification of arm movements using statistical and fuzzy techniques *Med. Eng. Phys.* **21** 303–11

Nishikawa D, Yu W, Maruishi M, Watanabe I, Yokoi H, Mano Y and Kakazu Y 2000 On-line learning based electromyogram to forearm motion classifier with motor skill evaluation *JSME Int. J.* C **43** 906–15

Parker P, Englehart K and Hudgins B 2006 Myoelectric signal processing for control of powered limb prostheses *J. Electromyogr. Kinesiol.* **16** 541–8

Perotto A, Delagi E F, Iazzetti J and Morrison D 2005 *Anatomical Guide For The Electromyographer: The Limbs And Trunk* (Springfield, IL: Charles C Thomas Publisher Ltd)

Phinyomark A, Limsakul C and Phukpattaranont P 2009 A novel feature extraction for robust EMG pattern recognition *J. Comput.* **1** 71–80

Sensinger J W, Lock B A and Kuiken T A 2009 Adaptive pattern recognition of myoelectric signals: exploration of conceptual framework and practical algorithms *IEEE Trans. Neural Syst. Rehabil. Eng.* **17** 270–8

Sun Y, Yu W, Han Z and Liu K J R 2006 Information theoretic framework of trust modeling and evaluation for *ad hoc* networks *IEEE J Sel. Areas Commun.* **2** 305–17

Van Trees H L 1968 *Detection, Estimation, and Modulation Theory* (New York: Wiley)

van Vugt J P and van Dijk J G 2001 A convenient method to reduce crosstalk in surface EMG. Cobb Award-winning article, 2001 *Clin. Neurophysiol.* **112** 583–92

Varol H A, Sup F and Goldfarb M 2010 Multiclass real-time intent recognition of a powered lower limb prosthesis *IEEE Trans. Biomed. Eng.* **57** 542–51

Vigreux B, Cnockaert J C and Pertuzon E 1979 Factors influencing quantified surface EMGs *Eur. J. Appl. Physiol. Occup. Physiol.* **41** 119–29

Williams T W 3rd 1990 Practical methods for controlling powered upper-extremity prostheses *Assist. Technol.* **2** 3–18

Zecca M, Micera S, Carrozza M C and Dario P 2002 Control of multifunctional prosthetic hands by processing the electromyographic signal *Crit. Rev. Biomed. Eng.* **30** 459–85

Zhou P, Lowery M M, Englehart K B, Huang H, Li G, Hargrove L, Dewald J P and Kuiken T A 2007 Decoding a new neural machine interface for control of artificial limbs *J. Neurophysiol.* **98** 2974–82